International Journal of
Molecular Sciences

MDPI

Article

Competing Easy Axis Anisotropies Impacting Magnetic Tunnel Junction-Based Molecular Spintronics Device (MTJMSD)

Bishnu R. Dahal,[1] Andrew Grizzle,[1] Christopher D'Angelo,[1] Vincent Lamberti,[2] and Pawan Tyagi*[1]

[1]Center for Nanotechnology Research and Education, Mechanical Engineering, University of the District of Columbia, Washington DC-20008, USA
[2]Y-12 National Security Complex, Oak Ridge, TN 37830, USA
* Correspondence: Author Email: *ptyagi@udc.edu*

Abstract: Molecular spintronics field's major challenge is the lack of mass-fabrication methods producing robust magnetic molecule connections with magnetic electrodes with different anisotropy. The another main challenge is the limitations of conventional theoretical methods for understanding experimental results and designing new devices. Magnetic tunnel junction-based molecular spintronics devices (MTJMSDs) are designed by covalently connecting the paramagnetic molecules across an insulating tunneling barrier. The insulating tunneling barrier serves as a mechanical spacer between two ferromagnets (FM) electrodes of tailorable magnetic anisotropies to allow molecules to manifest many intriguing phenomena. Our experimental studies showed that the paramagnetic molecules could produce strong antiferromagnetic coupling between two FM electrodes leading to a dramatic large-scale impact on the magnetic electrode itself. Recently we showed the Monte Carlo Simulation (MCS) was effective in providing plausible insights for the observation of unusual magnetic domains based on the role of single easy-axis magnetic anisotropy (Bishnu et al., Sci. Reports.,2022, Vol 12, 5721). Here we experimentally show that response of a paramagnetic molecule is dramatically different when connected to FM electrodes of different easy axis anisotropies. Motivated by our experimental studies, here we report a MCS study to investigate the impact of the simultaneous presence of two easy axis anisotropies on the MTJMSD equilibrium properties. In-plane easy axis anisotropy produced multiple magnetic phases of opposite spins. The multiple magnetic phases vanished at higher thermal energy, but MTJMSD still maintained a higher magnetic moment because of anisotropy. The out-of-plane easy axis anisotropy caused a dominant magnetic phase in the FM electrode rather than multiple magnetic phases. The simultaneous application of equal magnitude in-plane and out-of-plane easy axis anisotropies on the same electorate negated the anisotropy effect. Our experimental and MCS study provides insights for designing and understanding new spintronics-based devices.

Keywords: Magnetic tunnel junctions; single molecule magnets; Monte Carlo simulations; spintronics; anisotropy

1. Introduction

It's been over a decade since electron spin debuted in the semiconductor device industries [1-3]. The new field of electronics, called spintronics, harnesses the intrinsic spin of the electron and its associated magnetic moment along with electronic charge[4]. Spintronics has already revolutionized computer memory devices[5]. Spintronics possesses an inestimable potential for futuristic computer technology, including the development of quantum computers [6] and combining logic and memory in the same device[3, 7]. A significant limitation of the emerging technology is that it is based on limited traditional materials such as inorganic metals and semiconductors. Utilization of

the ferromagnetic metal is essential because of the high Curie temperature required for commercially useful applications[2, 8]. Alloying magnetic materials or stacking multiple magnetic layers offer possibilities of obtaining various magnetic properties[9, 10].

A new spintronics field is emerging that combines the quantum properties of the mass-producible molecule as the device element[11-13] between two ferromagnetic electrodes [14, 15]. Connecting molecules between two ferromagnetic electrodes opens a flood gate of innovations. Interestingly, commercially successful magnetic tunnel junction (MTJ) technology comes very close to the concept of connecting ferromagnetic electrodes with molecules as active transport channels. However, unlike the MTJ, which only rely on magnesium oxide like limited options for insulator[10] for desirable switching attributes [1, 9], molecule-based spintronics has almost billions of types of molecules to be included as spin channels. Molecules can be designed with useful optical, magnetic, and electrical properties. Most importantly, a desirable molecule can be mass-produced to sub-angstrom level structural precision[16-19].

Molecular spintronics devices (MSDs) can overcome the miniaturization limits and heating issues associated with the existing computer technology[20]. However, due to the nanoscale size of the molecules (~ 1 nm), it is difficult to maintain the molecular dimension robust and reproducible gap between the two ferromagnetic leads[21]. To avoid these difficulties, we developed a new approach to making magnetic tunnel junction-based molecular spintronics devices (MTJMSDs). To produce MTJMSD, the molecular channels were bridged across the insulator of an MTJ testbed with exposed side edges of FM electrodes. MTJMSD properties and their applications are highly influenced by ferromagnetic electrodes' physical properties, such as various anisotropies, thermal energy, coupling of ferromagnetic electrode atoms of two electrodes via the magnetic molecules, etc. [22]. Interestingly, we observed a remarkable difference between on and off-state with MTJMSD[23]. However, this observation was transient and insufficient to yield repeatable switching at room temperature.

Under the aspiration of making bistable memory devices, we experimentally realized MTJMSD by including two multi-layered magnetic electrodes with different magnetic properties deposited by the sputtering process. Prior literature shows that the simple addition of seed layers and just altering the sequence of thin ferromagnetic layers dramatically impact the magnetization properties of electrodes and devices [24-28]. Here we discuss experimental studies showing the impact of various magnetic electrodes on MTJMSD. Cross junction-shaped MTJMSD designed for conducting transport study possessed long ferromagnetic electrodes. Long ferromagnetic electrodes allow the connection of molecule-ferromagnetic electrode interfaces with the outer world for transport and device attributes. However, understanding the impact of the interaction between paramagnetic molecules and long multilayered ferromagnetic electrodes was experimentally challenging. The challenge of understanding MSD is harder when ferromagnetic electrodes possess different magnetic anisotropies. It is a daunting task to understand the overall device properties of MTJMSD experimentally when individually in-plane and out-of-plane easy-axis anisotropies are operating. Here we also present our Monte Carlo simulations (MCS) of MTJMSD with extended electrodes with variable anisotropies. In the MCS study, we systematically applied the in-plane and out-of-plane anisotropies individually and together to gain an atomistic understanding of resultant equilibrium properties.

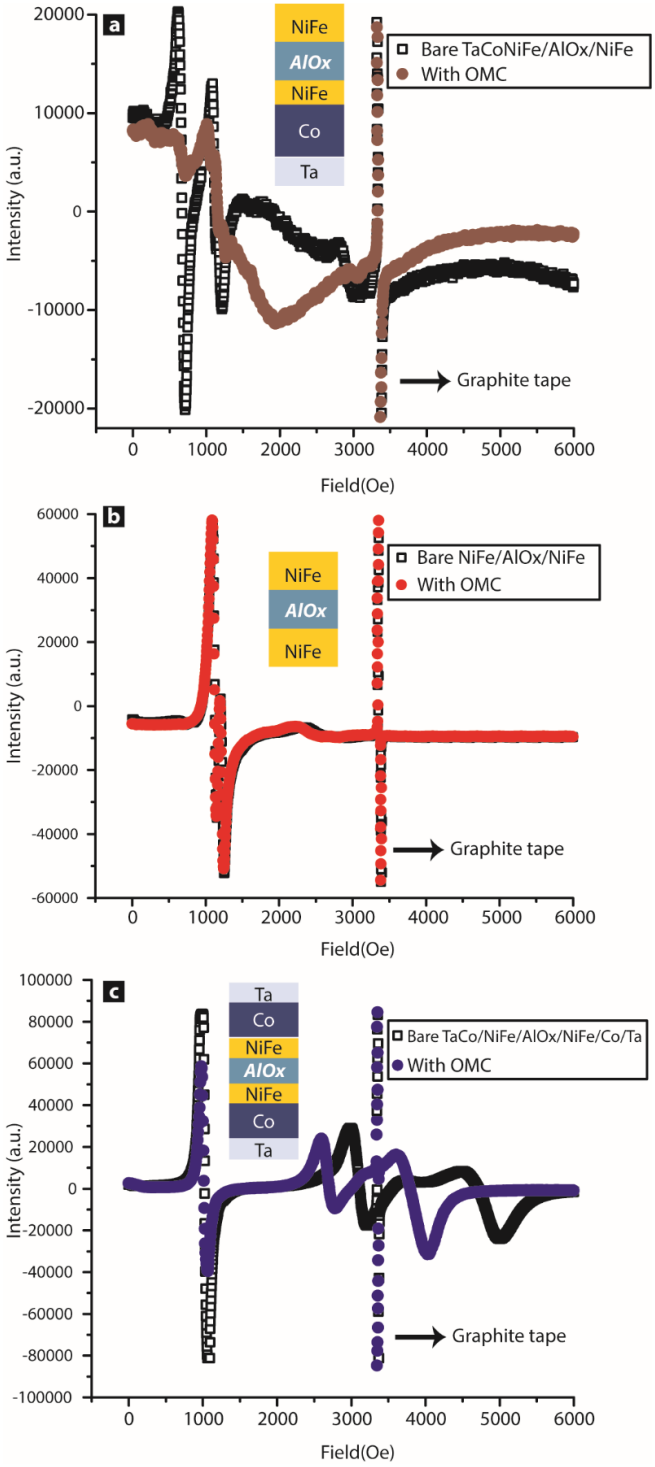

Figure. 1: FMR study before and after OMC treatment of ~7000 MTJS/sample with (a) Ta/Co/NiFe/AlOx/NiFe, (b) NiFe/AlOx/NiFe, and (c) Ta/Co/NiFe/AlOx/NiFe/Co/Ta thin film configuration.

2. Experimental Observations:

We experimentally produced pillar-shaped MTJ to investigate the effect of the difference in multilayer electrodes on the equilibrium properties of MTJMSD. In our prior work, we described the process of MTJ fabrication and the method of transforming it into MTJMSD by bridging molecules along the exposed side between two ferromagnetic electrodes [29]. Pillar-shaped MTJMSD brings distinctive advantages in that the ferromagnetic electrode is exactly confined within the perimeter of the tunnel junction area and molecular junctions. Hence, no interference or impact of ferromagnetic electrodes beyond the junction area will occur. The MTJ were patterned and deposited on silicon substrate with ~ 300 nm silicon dioxide layer. Each of the ~7000 cavities for producing MTJ pillars were photolithographically defined to be ~ 25 μm² area. All the MTJ layers were sequentially deposited in the cavities. The bottom electrode was deposited as a bilayer of ~ 5 nm cobalt (Co) and 5 nm NiFe. A ~ 2 nm tantalum seed layer was used for promoting adhesion between Co and silicon dioxide insulating layer. In the photoresist cavity sequentially, a 2 nm thick alumina (AlOx) and a ~10 nm thick NiFe top electrode were deposited. Utilization of the same photoresist cavity for all depositions ensured that the bottom FM electrode, ~2 nm AlOx, and the top FM electrode have the exact same lateral dimensions; this provision ensured that minimum physical separation between the top and bottom electrode would be equal to insulating thickness along the exposed side edges. The photoresist can be easily removed during the liftoff process to provide clean edges for bringing molecules of interest in the contact of two metal electrodes. The liftoff was accomplished to remove excess materials and produce Ta/Co/NiFe/AlOx/NiFe MTJ with an exposed side. Along the exposed side edges, organometallic molecular clusters (OMCs) or Single Magnetic Molecule (SMM) [30] were bridged across the AlOx

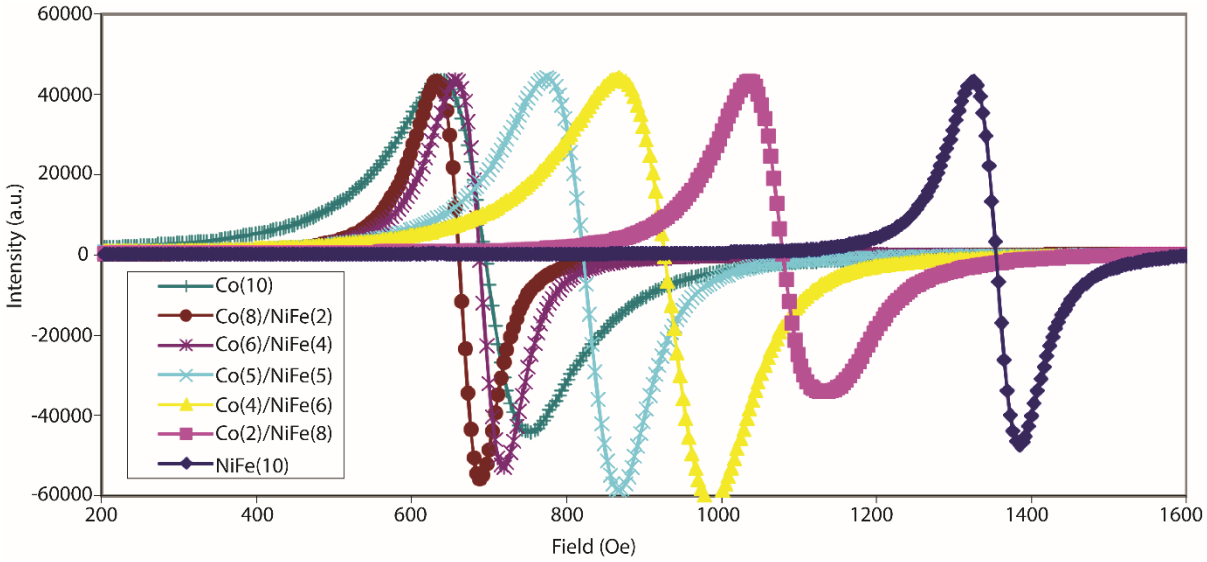

Figure 2: FMR study of Co/NiFe 10 nm thick bilayer with varying thickness of Co from 0 to 10 nm.

to complete the MTJMSD fabrication. In-depth details about OMCs properties in an as-produced state are published elsewhere [30, 31]. We utilized an electrochemical process for molecular self-assembly that is known to produce good metal-thiol bonding quickly. An OMC possessed cyanide-bridged octametallic molecular cluster, $[(pzTp)Fe^{III}(CN)_3]_4[Ni^{II}(L)]_4[O_3SCF_3]_4$ [(pzTp) = tetra(pyrazol-1-yl)borate; L = 1-S(acetyl)tris(pyrazolyl)decane] chemical structure. The internal exchange coupling between metallic ions in the OMCs exhibited an S=6 spin state in the bulk powder form at <10 K. It is extremely challenging to determine the actual OMC spin state when covalently bonded between two ferromagnetic electrodes in an MTJMSD. However, room temperature observations of the spin-photovoltaic effect[32], current suppression[33],

and other phenomena[23] assert that OMC could maintain a net magnetic spin state at room temperature.

As shown in Fig.1a, OMC significantly impacted the FMR modes of Ta/Co/NiFe/AlOx/NiFe MTJs. Acoustic mode (bigger peak) and optical mode (smaller resonance peak) on bare MTJ pillars were absent after bridging OMC channels. OMCs produced strong exchange coupling between two FM electrodes [29]. The bottom electrode containing cobalt was magnetically harder than the NiFe electrode in the present case. Our prior work demonstrated the difference in NiFe and Ta/Co/NiFe electrodes and multiple experimental evidence showing that OMC produced unprecedented strong inter-electrode antiferromagnetic coupling [29]; we are unsure if spin fluctuations has contributed in enhancing the impact of molecular channels similar to previous studies[14]. Interestingly, the same OMC molecule did not produce a noticeable impact on MTJ pillars with NiFe/AlOx/NiFe (Fig.1b). In this case, NiFe possessed in-plane easy axis. This MTJ sample with identical NiFe electrodes also showed acoustic and optical mode positions very close to each other, as compared to the case shown in (Fig.1a). In the third case, we treated Ta/Co/NiFe/AlOx/NiFe/Co/Ta CoNiFe pillars with OMCs. The role of Co in this case is to produce out of plane easy axis anisotropy and increase the overall magnetic hardness(coercivity) of the FM electrodes. Interestingly, this sample with both harder FM electrodes was impacted by OMCs (Fig.1c). Acoustic mode amplitude decreased due to the establishment of OMC channels. However, the optical mode (low amplitude mode) shifted towards the acoustic mode (Fig.1c). We do not have a clear understanding of the mechanism behind the observation and further work is in order for better understanding. However, the main conclusion of these experimental studies is the following: (a) OMC impact dramatically differs on MTJs with ferromagnetic electrodes of different magnetic hardness. (b) Ta/Co/NiFe also exhibited an FMR response in the out-of-plane magnetic field due to the presence of Co, whereas NiFe only responded to the inplane field during the resonance study. It means OMC's strong response on MTJ occurs when at least one FM electrode possesses an out-of-plane anisotropy. (c) OMC has severely impacted original FM electrodes and transformed them into different materials. Hence, the resultant MTJMSD is expected to have different top and bottom electrode magnetic anisotropy in this multilayer state.

We also conducted an FMR study on bilayer ferromagnetic thin films with variable Co and NiFe composition (Fig. 2). It is noteworthy that 10 nm Co and bilayer containing Co(8-6 nm)/ NiFe (2-4 nm) configurations responses were quite similar (Fig. 2). It means Co/NiFe bilayer with ≥ 6 nm Co will be dominated by the out of plane easy axis for magnetization. Bilayer with ≤ 5 nm Co thickness starts drifting towards NiFe dominated response that is governed by the in-plane easy axis. This FMR study does not intend to provide a quantitative analysis of anisotropy in bilayers. This study mainly suggests the wide range of possibilities when two easy axis may be present in the same magnetic electrode.

Magnetic electrodes with multiple anisotropies are a strong contender for developing novel devices and systems patterned in different forms. Cross-junction device architecture has been envisioned for MRAM application [34]. In cross-junction geometry, magnetic electrodes are expected to extend beyond the junction. We have extensively studied cross-junction shaped MTJMSD with 10 nm thick Co/NiFe bilayer electrode as the bottom electrode and ~10 nm thick NiFe top electrode. Our prior research has produced multiple pieces of evidence showing OMC's dramatic impact on the transport and optical properties of FM electrodes[23, 33, 35]. MTJMSD cross-junction shaped device geometry will need extended electrodes (Fig. 3a) around the junction to establish the connection between the molecular junction and the outer world (Fig. 3b). We observed that OMC molecules responded very differently for NiFe/AlOx/NiFe vs. Co/NiFe/AlOx/NiFe. In the case of NiFe/AlOx/NiFe, charge transport simply increased after connecting OMC channels along the edges (Fig. 3c). On the other hand,

cross-junction shaped MTJ with Co/NiFe/AlOx/NiFe resulted in non-linear tunneling in the bare state (Fig. 3d) and stabilized into ~ 6 orders of magnitude lower suppressed current state at room temperature (Fig. 3e). The difference in transport properties of NiFe/AlOx/NiFe and Co/NiFe/AlOx/NiFe after OMC treatment (Fig.3c-e) resembles with FMR response in Fig.1a-b. It is apparent that a slight difference in electrode composition has yielded a dramatic difference in OMC response. According to our prior work, OMC generally created strong antiferromagnetic coupling between the Co/NiFe and NiFe electrodes. Device fabrication details and other experimental information about cross-junction-shaped MTJMSDs are published elsewhere [32].

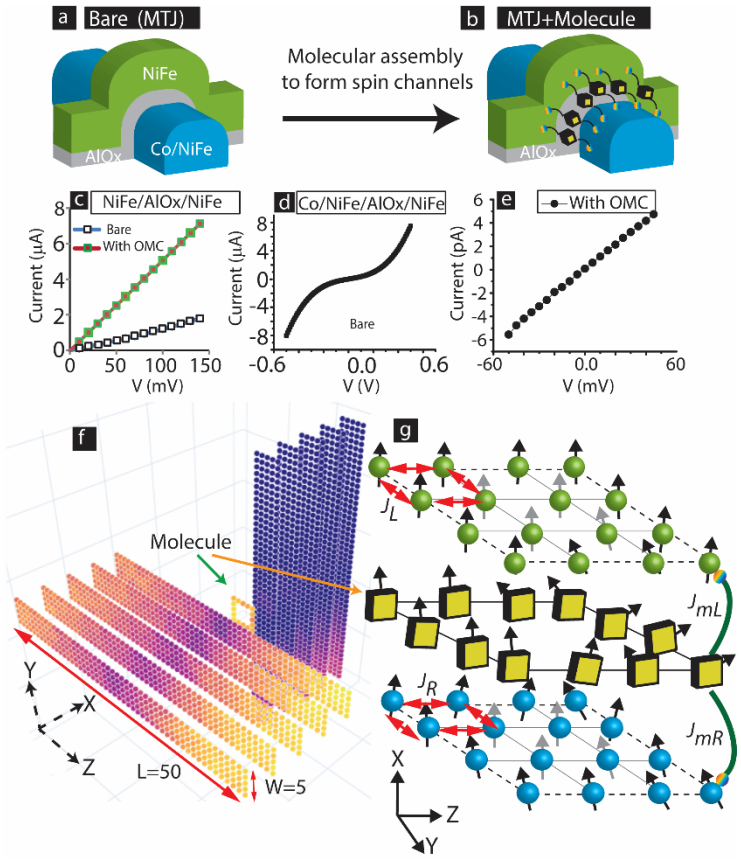

Figure 3. 3D sketch of cross junction shaped Magnetic Tunnel Junction (a) before and (b) after connecting molecular channels between two ferromagnetic electrodes. (c) NiFe/AlOx/NiFe I-V before and after interacting with molecules. I-V of Co/NiFe/AlOx/NiFe (d) in bare state and (e) after interacting with OMC molecules. (f) 3D atomic model of molecular device analogous to MTJMSD shown in panel (b). (g) Description of coupling energy around molecular junction of 3D model shown in panel (e).

A comprehensive study of the wide range of anisotropy magnitude in one electrode on the cross-junction form of MTJMSD is a daunting task via conventional DFT or micromagnetic methods. Hence, we have focused on the MCS study that allows us variation in cross-junction-shaped device geometry that involves thousands of atoms for computation with desktop lab computers. To encompass a wide range of possibilities about the various magnitudes of magnetic anisotropies of the two electrodes on MTJMSD, we have varied the in-plane easy axis anisotropy and the out-of-plane easy axis anisotropy parametrically. We envisioned that each combination may represent a new case in a futuristic experimental study and may be understood with the help of the MCS study discussed here.

3. Computational Methodology:

This manuscript mainly focuses on the Monte Carlo Simulation (MCS) study of MTJMSD. We varied two easy-axis anisotropies in only one FM electrode to make the MCS study relevant to the experimentally studied cross-junction-shaped MTJMSDs with one bilayer FM electrode. We also focused on only one FM electrode to extend the insights shared in our recent publications about the impact of only one easy axis direction in one FM electrode[36]. In our study, only the right FM electrode is isotropic, but in-plane and out-of-plane easy-axis anisotropies were applied on the left FM electrode. All other parameters except thermal energy (kT) that can impact the overall magnetic properties of MTJMSD were kept constant during the MCS. To be consistent with the experimental scenarios, we had adopted the case when molecules produced strong antiferromagnetic coupling with one FM electrode and ferromagnetic coupling with another FM electrode [21]. Magnetic tunnel junction (MTJ) with cross junction geometry is shown in the bare state (Fig. 3a) and with molecules on the edges (Fig.3b). The schematic description of the dimension of MTJMSD, including the spin orientation of molecules and FM atoms were described elsewhere [21]. We designed a 3D Heisenberg model to represent cross junction-shaped devices (Fig. 3f). The Hamiltonian for computing MTJMSD's energy during MCS is shown in equation 1.

$$E = -J_L\left(\sum_{i\in L}\vec{S}_i\vec{S}_{i+1}\right) - J_R\left(\sum_{i\in R}\vec{S}_i\vec{S}_{i+1}\right) - J_{mL}\left(\sum_{i\in L, i+1\in mol}\vec{S}_i\vec{S}_{i+1}\right) - J_{mR}\left(\sum_{i-1\in mol, i\in R}\vec{S}_{i-1}\vec{S}_i\right) - A_{Lx}\left(\sum_{i\in L}\vec{S}_i^2\right) - A_{Ly}\left(\sum_{i\in L}\vec{S}_i^2\right) \quad \text{(Eq.1)}$$

The size of the MTJMSD Heisenberg model in this MCS study is confined in the box of $HxWxL$ (=11×50×50) volume in atomic units. Here, H, W, and L are atomic height, width, and length, respectively. In this model, FM electrodes are of 5x5x50, and molecules are represented by 5x5 square with an empty interior as shown in Figure 3f. Empty interior represents the AlOx-like insulator needed in MTJMSDs to ensure a molecule scale spacing between the two FM electrodes. In equation(1), S_i represents the spin of FM atoms and molecules. The S_{i+1} and S_{i-1} symbols represent the nearest neighbors with respect to spin at the ith site. The Heisenberg coupling across the ferromagnetic atoms of left and right electrodes, represented by J_L and J_R , always kept to their maximum values, i. e. $J_L = J_R = 1$ during the MCS (Fig. 3g). Similarly, J_{mL} represents the Heisenberg coupling of molecules with the atoms of left FM electrodes while J_{mR} represents the Heisenberg coupling of molecules with the atoms of right FM electrodes. To maintain the antiferromagnetic coupling of molecules with left and right FM electrodes, we fixed the values of $J_{mL} = -1$ and $J_{mR} = 1$, as illustrated in Figure 3g.

In our previous research, we experimentally estimated the strength of molecule-induced exchange coupling [21]. We conducted a temperature vs. MTJMSD magnetic moment study and observed the molecule-induced strong exchange coupling breakdown ~400 K. This temperature is popularly known as Neel temperature(T_N) in the case of antiferromagnets [21]. The presence of T_N affirmed that OMCs induced a net antiferromagnetic coupling between the two FM electrodes. To compute the relative energy needed to

break OMC induced bonding we compared the OMC induced T_N with the Curie temperature (T_c) of the NiFe FM electrode. We focused on the NiFe ferromagnet because of the fact that only NiFe FM directly bonded with OMCs. As per prior literature NiFe exhibited T_c around 800 K [37]. We found that the T_N/T_C ratio was ~0.5 [21]. Based on the experimental studies we concluded that OMC induced antiferromagnetic coupling was of the order of 0.5 times of the interatomic ferromagnetic exchange coupling strengths. This indirect estimation of nature and strength of J_{mL} and J_{mR} is in accordance with the assumption that kT_c for a FM corresponds to the interatomic exchange coupling [38]. Since this MCS study cover a wide range of molecules and FM electrodes, we have surmised that J_{mL} and J_{mR} can be higher than what we computed and selected the magnitude to be 1. We also represented molecule with an atomic analog based on our recent research[39]. This simplified representation of molecule makes such MCS possible. We have showed that beyond a critical value of molecular spin (~0.2) variation in molecule spin state do not dramatically impact long range ordering on FM electrodes of an MTJMSD [39].

Under MCS approach the energy of the MTJMSD was minimized to reach the equilibrium state. During the simulation, the ambient thermal energy in which MTJMSD operate was represented by the kT. The kT factor play critical role in the Metropolis algorithm in producing stable MTJMSD configuration for each combinations of simulation parameters. MCS method has been discussed elsewhere [21]. In the present MCS study we fixed kT to 0.1. In practical term the kT = 0.1 correspond to the operational temperature that ranges from 50 °C to 130 °C after accounting for the internal computer heatings but close to room temperature. Our analogy is based on the assumption that the Curie temperature of various candidate FM electrodes can vary from 500 °C to 1300 °C[40].

We studied the impact of unidirectional out-of-plane anisotropy along an x-direction easy axis (A_{Lx}) and in-plane anisotropy along the y-direction easy axis (A_{Ly}) on the left FM electrode. We varied all the possible combinations for A_{Lx} and A_{Ly}. We varied the values of A_{Ly} from no anisotropy (A_{Ly} = 0) to its maximum value, i. e. A_{Ly} = 1 for all possible values of A_{Lx} (from A_{Lx} = 0 to 1 at the step of 0.1). To keep the discussion generic, the exchange coupling parameters, magnetic anisotropy, and thermal energy are referred to as the unitless parameters throughout this computational study.

4. Results and Discussions:

The first step in exploring the effect of anisotropy on MTJMSD focused on understanding focus on the evolution of the equilibrium state from the perturbed states. For this objective, we explored the evolution of MTJMSD with time for combinations for A_{Lx} and A_{Ly}. Figure 4 shows the impact of anisotropies on the overall magnetic properties of MTJMSD during energy minimization of MCS (Magnetic Moment Vs. iteration counts) with given in-plane and out-of-plane easy-axis anisotropies. Temporal evolutions were recorded at kT=0.1 . Figure 4a shows the variation of the magnetic moment of MTJMSD as a function of iteration counts when there were no anisotropies on the left ferromagnetic electrode. Based on the dimension of the MTJMSD used during MCS, the left ferromagnetic, and the right ferromagnetic electrodes can attain the maximum magnitude of the magnetic moment of 1250. At the same time, MTJMSD's maximum magnetic moment can settle around 2516 (1250 for each ferromagnetic electrode and 16 for molecules). It is noteworthy that we kept the right electrode isotropic during the simulation. As a result, the total magnetic moment of the right FM electrode is always close to its maximum value of ~1200. When A_{Lx} =0 and A_{Ly} = 0 the magnetic moment of the left electrode started to increase quasi-linearly with the iteration counts before it saturated around 250 million iterations. The magnetic moment of the left electrode saturated to its maximum value of ~1150. In the absence of anisotropies, the antiferromagnetic coupling provided by the Heisenberg coupling of left and right electrodes with the molecules was the dominating factor. The molecule coupling with electrodes was J_{mR} = 1 and J_{mL} = -1, respectively. The total magnetic moment of the MTJMSD was always lower than that of the left and the right electrodes due to the opposite magnetic spins of the left and the right FM electrodes (Fig. 4a). When A_{Lx} =0 but A_{Ly} =0.5 , the in-plane anisotropy forced to align the magnetic

spins of the left ferromagnetic electrode and overcame the effect of J_{mL} (Fig. 4b). It was also observed that the A_{Ly} caused the magnetic moment to align in the particular spin direction opposing J_{mL}.

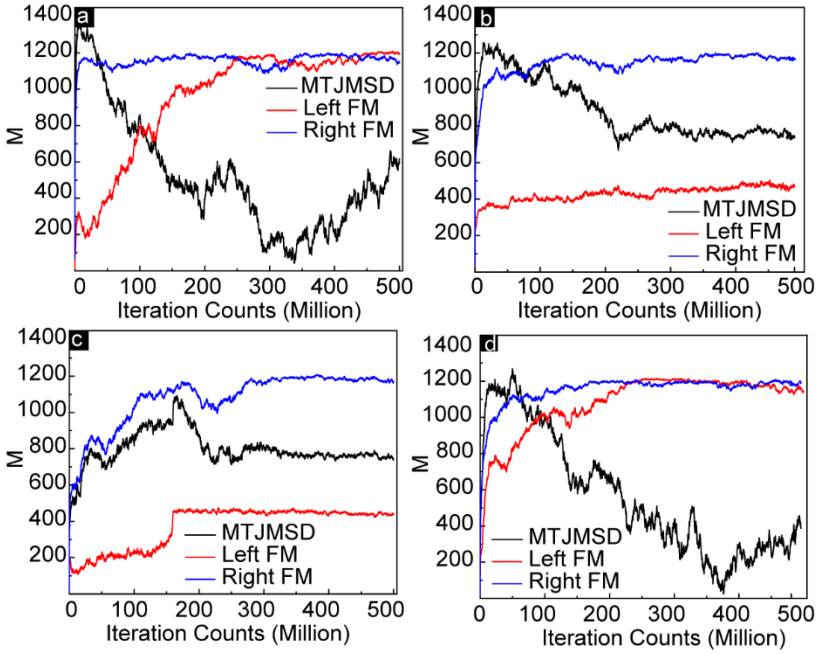

Figure 4: Temporal evolution of the MTJMSD, and two electrodes are measured by monitoring magnetic moment as a function of iteration counts(equivalent to simulation time) for (a) A_{Lx} =0 and A_{Ly} =0 (b) A_{Lx} =0 and A_{Ly} =0.5 (c) A_{Lx} =0.5 and A_{Ly} =0 and (d) A_{Lx} =1 and A_{Ly} =1.

As a result, the magnetic moment of the left electrodes was decreased, but that of MTJMSD increased. The impact of out-of-plane anisotropy and the competing effect of in-plane and out-of-plane anisotropy has described in Fig. 4c and Fig. 4d, respectively. When A_{Lx} =0.5 and A_{Ly} =0 (Fig. 4c), the impact of out-of-plane anisotropy was somewhat similar as provided with the equal magnitude of in-plane anisotropy (Fig. 4d).

A notable observation was around 175M iteration counts. At this stage, a sudden jump in the magnetic moment of the left FM electrode was observed (Fig. 4c). The sudden jump in the magnetic moment of the left FM electrode was due to the formation of the dominant magnetic phase of the same spin orientations due to the out-of-plane easy axis anisotropy which will be the part of further discussion of this manuscript. The magnetic moment saturates close to ~425 immediately after the sharp jump of the magnetic moment. With the application of in-plane and out-of-plane anisotropies on the same left ferromagnetic electrode, we observed that the effect of anisotropies started to annihilate each other (Fig. 4d). We defined the annihilation as the "competing impact" in this report. The competing impact of anisotropies helped to have a high value of magnetic moments by aligning all the magnetic spins of atoms of the left electrode. But the orientation of the magnetic spins of the left FM electrodes was opposite to that of the isotropic right electrode due to molecule-induced strong antiferromagnetic coupling. Therefore, the total magnetic moment of MTJMSD was observed to be smaller than that of the left and the right electrodes. When the magnetic moment of the left and right electrodes were closely equal, but the magnetic spins of left and right FM electrodes were opposite (~325 M iter-

ation counts), the total magnetic moment of MTJMSD was almost zero, as shown in **Fig. 4d**. The overall magnetic moment of MTJMSD was similar when anisotropies were not applied on the left FM electrode (**Fig. 4a**) or when the FM electrode has an equal magnitude of in-plane and out-of-plane anisotropies (**Fig. 4d**). The prior case happened due to the antiferromagnetic Heisenberg coupling of the left and the right FM electrode with paramagnetic molecules. In comparison, the latter case was due to the competing effect of in-plane and out-of-plane anisotropies on the left FM electrode.

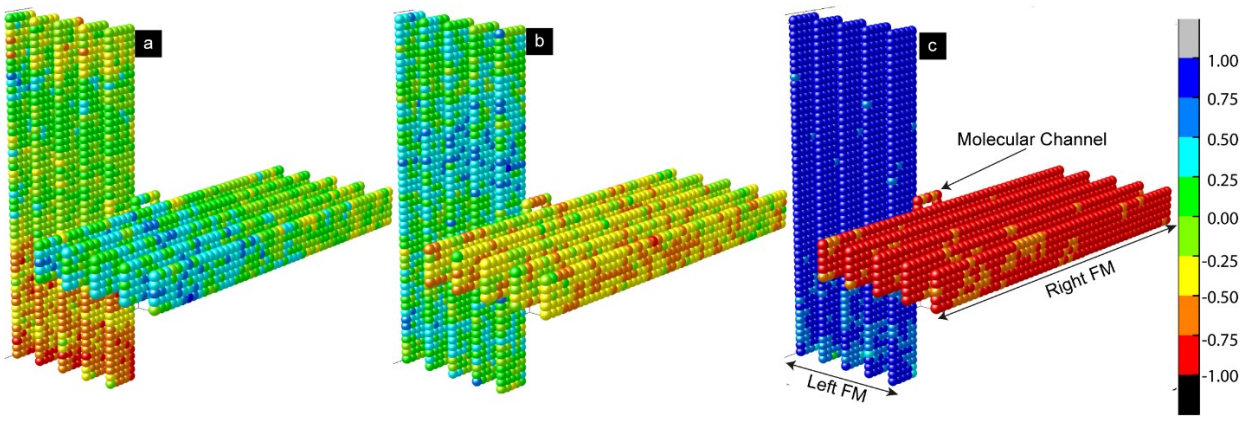

Figure 5: Spatial 3D lattice model of the MTJMSD measured in the equilibrium state at the end of simulations at $kT = 0.1$, $A_{Lx} = A_{Ly} = 0$ along (a) spin direction X-axis, (b) spin direction Y-axis, and (c) spin direction Z-axis.

To understand the actual spin configurations of the left and right FM electrodes, we analyzed the atomic scale equilibrium moment of MTJMSD's Heisenberg model (**Fig. 5 and Fig. 6)**. Figure 5 shows three 3D spins vector intensities along x, y, and z directions. In 3D atomic schematic representation, the left FM electrodes are represented by vertical lattices while horizontal lattices represent right FM electrodes, and molecules are represented by small squares between left and right FM electrodes. The color scale bar presented in **Fig. 5 and Fig. 6** represents the normalized magnetic moment. A Monte Carlo simulation (MCS) takes the variable that has uncertainty and assigns it a random seed. The model is then run, and a result is provided. This process is repeated while assigning the variable in question with many different values. Once the simulation is complete by energy minimization, the equilibrium state magnetic moments are averaged together to provide an estimate. As a result, the settlement of the magnetic spins is always arbitrary along spin direction x or y or z-direction in the absence of anisotropies, as illustrated in **Fig. 5.** In this particular situation, the spins of magnetic atoms settled in the z-direction. The settlement of magnetic spins directions is completely random unless we provide the same seed or apply the anisotropies during the simulations. The closeness of the color corresponding to the magnetic moment of the molecules and the first right ferromagnetic electrode is because molecules made strong ferromagnetic coupling with the right electrode ($J_{mR} = 1$). On the other hand, the complete color contrast of molecules to the left ferromagnetic electrode is because the molecule made an antiferromagnetic coupling with the left electrode ($J_{mL} = -1$).

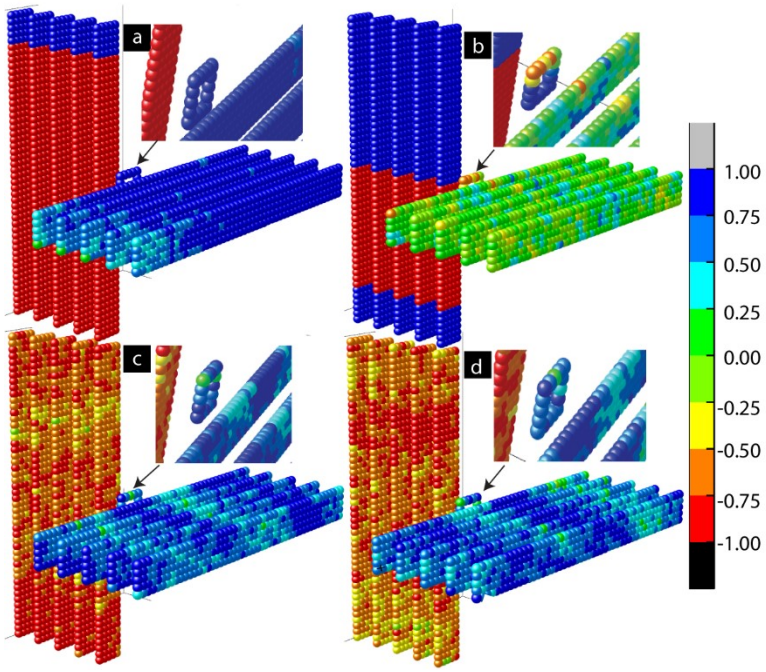

Figure 6: Simulated spatial 3D lattice model of the MTJMSD measured at $kT = 0.1$ (a) $A_{Lx} = 1$, and $A_{Ly} = 0$ (b) $A_{Lx} = 0$, and $A_{Ly} = 1$, (c) $A_{Lx} = 1$, and $A_{Ly} = 1$ along spin direction x-axis, and (d) $A_{Lx} = 0$, and $A_{Ly} = 0$.

Figure 6a represents the 3D lattice model along the x-spin direction when out-of-plane magnetic anisotropy A_{Lx} =1. Anisotropy causes the multiple magnetic domains of opposite spins that appear on the left ferromagnetic electrode (**Fig. 6a)**. These domains represent the different magnetic phases. With the application of strong out-of-plane anisotropy, a dominant magnetic phase appeared on the left electrode. A residual secondary magnetic phase of opposite spins also appeared, as shown in **Fig. 6a**. The effect of anisotropy appeared on the left ferromagnetic electrode and transferred to the right ferromagnetic electrode via molecular channels. As a result, ordered magnetic spins states appeared on the right electrode despite not having any anisotropies on the right FM electrodes ($A_{Rx} = A_{Ry} = 0$). The spin orientations of the right FM electrodes were opposite to that of the left FM electrode despite the spin stabilizations that happened to the right FM electrodes due to the left FM electrode. The molecules maintained the antiferromagnetic couplings with the left FM electrode represented by opposite spin colors red and blue for the left FM electrodes and molecules, respectively. Since the molecular exchange coupling were transferring the impact to the right FM electrodes via molecular channels, the spin orientations of the right FM electrodes aligned themselves to the molecules' spin directions. The application of in-plane anisotropy (A_{Ly}=1) caused the multiple magnetic phases of opposite magnetic spins, as shown in **Fig. 6b**. Unlike out-of-plane anisotropy, there was no dominant magnetic phase. Molecular channels were connected on the left electrode in the boundary region of two phases of opposite spins, as shown in **Fig. 6b**. As a result, the effect of anisotropy appearing on the left electrode cannot be transferred to the right electrode. When $A_{Lx} = A_{Ly}$ =1, the competing impact of in-plane and out-of-plane anisotropies were observed on the electrode, as shown in **Fig. 6c** and **Fig. 6d.** When we carefully observed the 3D lattice, **Fig. 6c**, slightly more red spots ap-

peared on the left electrode. This is because the net magnetic moment caused by the dominant magnetic phase on the left electrode was not destroyed due to the competing impact.

We also investigated the effect of thermal energy (kT) on MTJMSD for various combinations of anisotropies. Figure 7 represents the magnitude of magnetic moment measured continuously as a function of anisotropy at constant thermal energies. We varied the thermal energy kT = 0.1 to 1. Thermal energy kT = 0.1 is near room temperature with the assumption that the Curie temperature of the MTJMSD varies with FM electrode from 300 °C to 800 °C. **Figure 7a** represents the contour plot for the magnetic moment of MTJMSD as a function of A_{Lx} and A_{Ly} measured at kT= 0.1. It is difficult to analyze the magnetic moment of the overall device without understanding the behavior of individual ferromagnetic electrodes. It is also very challenging to idintify the regions with in-plan and out of plane magnetic phases that are natural outcome of in-plane and out of plane easy axis anisotropies, respectively[40]. Therefore, we first focused on analyzing the effects on the individual ferromagnetic electrode. Figure 7b represents the plot for the magnetic moment of the left ferromagnetic electrode as a function of A_{Lx} and A_{Ly} measured at kT= 0.1. It is interesting to note that the magnetic moment of the left FM electrode remains high, varies from 1200 to 1250, for the situation when $A_{Lx} \geq A_{Ly}$. A_{Lx} stabilize out-of-plane magnetic direction, represented by the red regime on the lower right of the contour diagram (Fig. 7b). Out-of-plane anisotropy (A_{Lx}) caused the formation of the big single magnetic domain of the same magnetic spin orientation. The big magnetic domain represented a single magnetic phase and was responsible for keeping the higher magnetic moment along the out of plane x direction. In this case where A_{Lx} is dominant magnetic domain's direction will be parallel or antiparallel to out of plane x direction. The higher magnetic moments due to the single magnetic domain was consistently observed in the 3D lattice model, as shown in Fig. 6a. In the diagonal region, when $A_{Lx} = A_{Ly}$, the magnetic moment of the left ferromagnetic electrode is slightly lower than the case when $A_{Lx} \geq A_{Ly}$ and remains nearly constant, as illustrated by the orange stripe in Fig. 7b. The smaller values of magnetic moments are due to the multiple magnetic phases of opposite spins that appeared in the left ferromagnetic electrodes due to the application A_{Ly}. It is also anticipated that left FM electrode switches from out of plane to in-plane magnetic direction for $A_{Lx} \leq A_{Ly}$. The formation of multiple magnetic phases of opposite spins on the same left ferromagnetic electrode due to the application of in-plane anisotropy (A_{Ly}) is also illustrated in Fig. 6b. However, in this case where A_{Ly} is dominant magnetic domain's direction will be parallel or antiparallel to in plane y direction.

The magnetic moment on the right FM electrode was relatively high compared to that of the left ferromagnetic electrode since we had not applied any anisotropies on the right ferromagnetic electrode (Fig.7c). But, when we carefully observed the contour plot, there was a general trend for the values of the magnetic moment. For the right ferromagnetic electrode, the magnetic moment was lower in the region $A_{Lx} \geq A_{Ly}$ compared to that of the region $A_{Lx} \leq A_{Ly}$. As we discussed in Fig. 7b, the effect of molecular exchange coupling from the left ferromagnetic electrode can transfer to right electrode via molecular channels. This molecular exchange coupling was responsible for creating moderately aligned magnetic spins in the right electrode even if we did not apply magnetics anisotropies on the right electrode, Fig. 7c. Most importantly, molecular coupling play major role in setting magnetic spin direction on right FM electrode in accordance to the left FM electrode. The right FM electrode magnetization will be in plane or out of plane based on what easy axis anisotropy is dominating the left electrode. In essence strong antiferromagnetic molecular coupling role is to set the FM electrode spin orientation opposite to the spin orientation on the left FM electrode. The diagonal region has small variations of magnetic moment, varying from 1080 to 1120. The magnetic moment of MTJMSD was the overall sum of magnetic moments of the left ferromagnetic electrode, the right ferromagnetic electrode, and molecules.

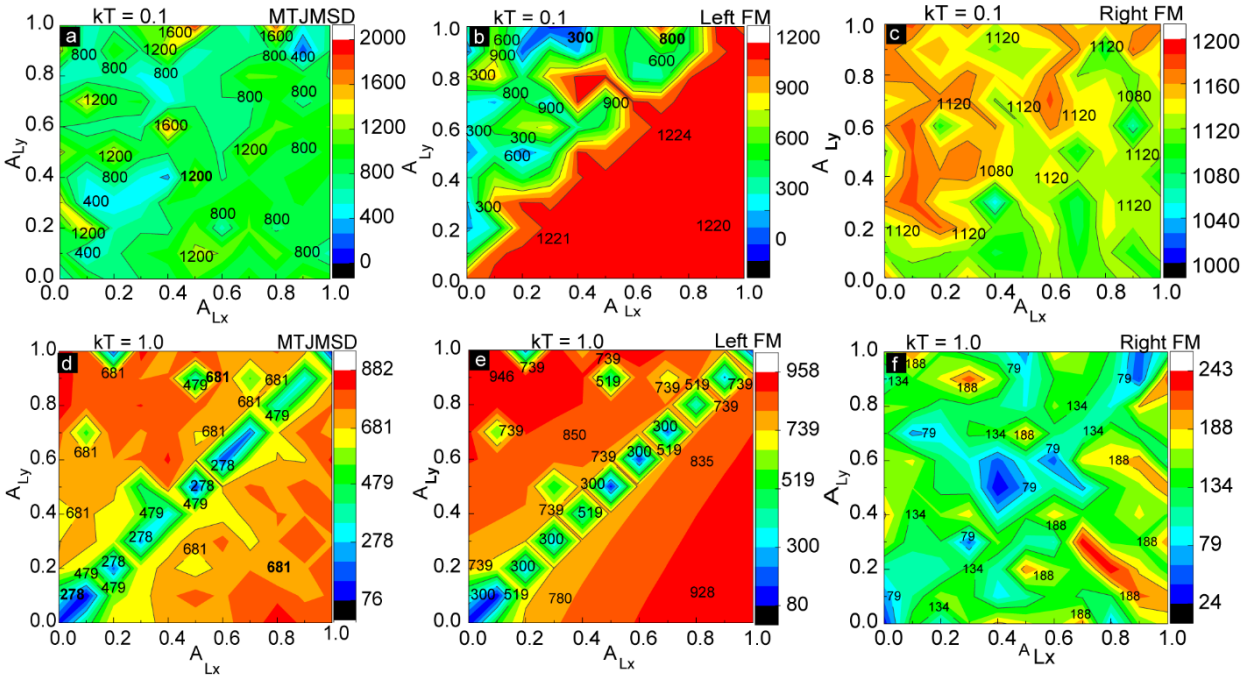

Figure 7: Magnetic moment as a function of in-plane (A_{Ly}) and out-of-plane (A_{Lx})anisotropies at kT=0.1 for (a) MTJMSD , (b) left ferromagnetic electrode at, (c) right ferromagnetic electrode at. Magnetic moment as a function of in-plane (A_{Ly}) and out-of-plane (A_{Lx})anisotropies at kT=1 for(d) MTJMSD at (e) left ferromagnetic electrode (f) right ferromagnetic electrode.

As the temperature increased, thermal energy started to annihilate the magnetic domains. Here we discuss the magnetic moments of MTJMSD (Fig.7d), left electrode (Fig.7e), and right electrode (Fig.7f), respectively measured at kT = 1. In the diagonal region, the region with $A_{Lx} \approx A_{Ly}$, the in-plane and out-of-plane anisotropy had a competing effect. As a result, the region had a small value of net magnetic moment compared to both $A_{Lx} \leq A_{Ly}$ and $A_{Lx} \geq A_{Ly}$ regions. It is noteworthy that $A_{Lx} \approx A_{Ly}$ represent the case where four directions are possible and this scenario is similar to when no anisotropy is active. As an analogy, zero force on a point is equivalent to equal and opposite forces on the same point. High temperature annihilated the magnetic phases of opposite magnetic spins along in plane y easy axis and out of plane x easy axis. Therefore, unlike to kT= 0.1, magnetic moments were nearly symmetric in both $A_{Lx} \leq A_{Ly}$ and $A_{Lx} \geq A_{Ly}$ regions as shown in Fig. 7d. Because of high thermal agitation, molecular exchange coupling could not transfer from the effect of anisotropy on the left electrode to the right electrode via molecular conducting channels (Fig.7f). The right electrode without anisotropy underwent from ferromagnetic to paramagnetic state after increasing the thermal energy close to curie temperature (Fig. 7f). So, magnetic spins on the right electrode were randomly orientated. The magnetic moments of the left FM electrode (Fig. 7e) was significantly more than that of right FM electrode (Fig. 7f) for kT=1. It is interesting to note that magnetic spins were still in the moderately ordered state even at Curie temperature (kT= 1.0) because of in-plane and out-of-plane anisotropies. But the overall magnetic moment of MTJMSD (Fig. 7d)is less than that of the left electrode (Fig. 7e) due to the irregular orientations of magnetic spins at high thermal energy.

We further investigated the length scale of different phases in ferromagnetic electrodes and spatial correlation between molecular spins and FM electrodes (**Fig. 8**). To quantify the correlation of spins between molecules and atoms in different layers of the ferromagnetic electrodes in the presence of in-plane and out-of-plane anisotropies, we have studied the customized spatial correlation factor (*SC*). *SC* is the dot product between average molecular spin vector and the of spin vectors in each atomic row of two ferromagnetic electrodes. The equation used to calculate the *SC* is as follows(equation 2):

$$SC = (S_m\vec{x} + S_m\vec{y} + S_m\vec{z}).(S_{FM}\vec{x} + S_{FM}\vec{y} + S_{FM}\vec{z}) \quad \text{(Eq.2)}$$

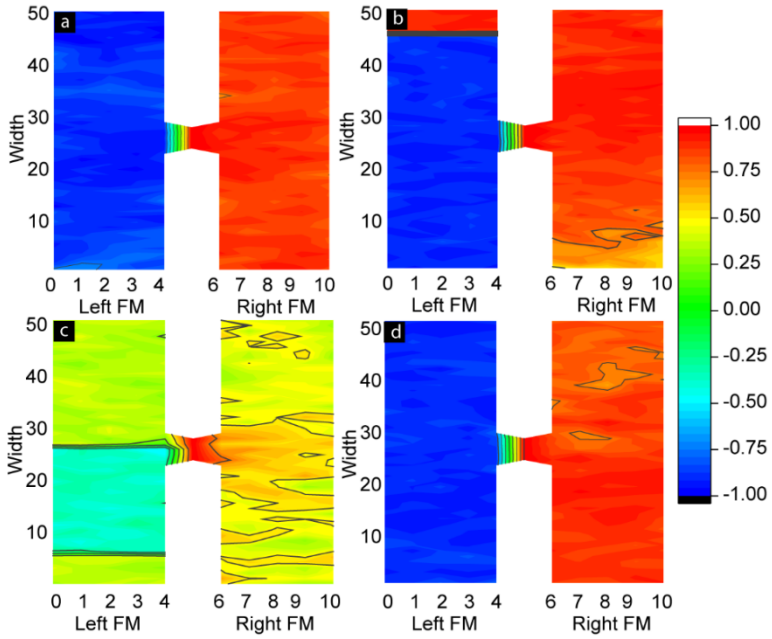

Figure 8: Spatial correlation (SC) factor contour plots of MTJMSD at kT = 0.1 with (a) $A_{Lx} = A_{Ly} = 0$, (b) $A_{Lx} = 1$ and $A_{Ly} = 0$, (c) $A_{Lx} = 0$ and $A_{Ly} = 1$, and (d) $A_{Lx} = A_{Ly} = 1$.

Positive *SC* represents the parallel alignment of spins of ferromagnetic atoms with the spins of molecules. Negative *SC* represents the antiparallel alignment of the magnetic moment of atoms of the left and right ferromagnetic electrode with molecular spins. The magnitude of *SC* suggests the strength of correlation between molecule and FM electrode layers. The SC contours shown in Figure 8 correspond to the cases of anisotropy shown in 3D lattice plots Figure 6. Here, Fig. 8a is for $A_{Lx} = A_{Ly} = 0$, Fig. 8b for $A_{Lx} = 1$ and $A_{Ly} = 0$, Fig. 8c for $A_{Lx} = 0$ and $A_{Ly} = 1$, and Fig. 8d for A_{Lx} and $A_{Ly} = 1$. When $A_{Lx} = 0$ and $A_{Ly} = 0$, the spin states of two ferromagnetic electrodes are highly correlated with the spin states of the molecules. Molecule-induced strong antiferromagnetic coupling forced left FM and right FM electrodes to assume antiparallel states (Fig. 8a and Fig. 5c). Atomic Spins of left ferromagnetic atoms were negatively correlated with the molecular spins, while atomic spins of right ferromagnetic electrodes were positively correlated with the molecular spins. These correlations were expected in the MTJMSD Heisenberg model, since molecules were antiferromagnetically and ferromagnetically coupled with left and right FM electrodes, respectively. In the absence of anisotropies, the antiferromagnetic coupling of molecules with electrodes was dictated by $J_{mL} = -1$ and $J_{mR} = 1$ values. It is noteworthy that the segments of the molecules adjacent to the ferromagnetic electrodes tend to align their

spins in strong correlation with the spins of ferromagnetic electrodes, as shown in Fig. 8a, Fig. 8b, and Fig. 8d. When the molecular conducting channels are right on the magnetic phases transition region, multiple magnetic spins were also appeared on the molecular spin states, as shown in Fig. 6b and Fig 8c. Domain wall width of multiple magnetic phases also depends upon the anisotropy which is reported elsewhere. In-plane anisotropy causes the formation of multiple magnetic phases of opposite magnetic spins. But the high value of A_{Ly} caused the formation of the dominant magnetic domain in the left ferromagnetic electrode, represented by the red domain color in Fig 8b. Magnetic spins of this dominant region were negatively correlated with the molecular spins, and the region stood up to the 47th atomic layer of the left ferromagnetic electrode. The spatial correlation factor is ~-0.8 as shown in Fig. 8b.

A second magnetic domain is standing on 48th, 49th, and 50th atomic layers on the same left ferromagnetic electrode. This domain not only has opposite magnetic spins compared to the dominant magnetic region but also is positively correlated with the molecular magnetic spins with an equal magnitude of autocorrelation factor but with the opposite sign, i. e. ~0.8 As discussed previously, the out-of-plane anisotropy causes the multiple magnetic phases on the left ferromagnetic electrode (Fig. 8c). From atomic layers 0 to 8, magnetic spins are positively correlated with the molecular spin with the correlation factor~0.3. From layers 8 to 26, the magnetic spins are negatively correlated with the spin of the molecules, having a correlation factor around -0.35. From layers 27 to 50, magnetic spins are again positively correlated with the molecular spins with a correlation factor of ~0.3. It is noteworthy to mention that the anisotropy not only creates different magnetic phases of opposite spins but also these phases have spins correlated with molecular spins of equal magnitude but with opposite spin orientations. The right ferromagnetic electrode for this case stabilize in completely random direction (Fig. 8c). It is due to the reason that the anisotropy effect cannot transfer from the left to the right ferromagnetic electrode via the molecular conducting channel. This is because the molecular conducting channels fall in the region of phase transition. As a result, molecular spins are positively correlated with the spins of an electrode and negatively correlated with another electrode. In the present case when both anisotropies are existing, molecular spins are positively correlated with the magnetic spins of the right ferromagnetic electrode, while they are negatively correlated with the magnetic spins of the left electrode (Fig. 8d). The left electrode exhibited single phase unlike the cases of appearance of multiple phases observed for unequal in-plane and out-of-plane anisotropies.

6. Conclusions

This paper discussed the impact of various anisotropy nature on MTJMSD. We gained the following insights.

1. We experimentally showed that variation in the plane and out-of-plane easy axis of the ferromagnetic electrodes connected to exactly the same paramagnetic molecular channels yielded dramatically different equilibrium properties.
2. MTJMSD offers unprecedented opportunities to innovate novel spintronics devices by simple variation in thin film electrode layers. Our FMR study showed that a 10 nm thick bilayer of Co/NiFe yielded significant differences in magnetic properties for the different ratios of Co and NiFe thickness.
3. Cross junction-shaped MTJMSD is a strong candidate for cross-bar geometry-dependent logic and memory devices proposed in prior literature. Our initial transport studies with cross-junction-shaped MTJMSD showed that variation in FM electrode anisotropy yielded a

dramatically different response. Our experimental study necessitated the investigation of a wide range of magnetic anisotropies on MTJMSD. We adopted MCS methodologies due to their distinctive advantage in handling complex MTJMSD requirements.

4. We focused on Monte Carlo Simulation (MCS) to analyze the variation of the magnetic moment as a function of iterations, anisotropies, and thermal energy. During the MCS study, we applied in-plane and out-of-plane anisotropies on the left ferromagnetic electrode while keeping the right ferromagnetic electrode isotropic.
5. We observed that the presence of in-plane anisotropy caused the multilayer magnetic phases on the same ferromagnetic electrode of the magnetic tunnel junction (MTJ). These multiple magnetic phases of opposite spins behave as soft and hard magnetic phases. The strong magnitude of out-of-plane anisotropy resulted in a dominant magnetic phase on the ferromagnetic electrode so that the magnetic moment of overall MTJMSD was higher for the region $A_{Lx} \geq A_{Ly}$.
6. The simultaneous application of in-plane and out-of-plane anisotropies starts to negate the overall anisotropy properties. The electrode was completely isotropic when $A_{Lx} = A_{Ly}$.The computationally analyzed magnetic properties of MTJMSD will provide deep insight into the future experimental study of molecular spintronics and molecular-based magnetic tunneling junction devices.
7. Our experimental studies highlight the unique attributes of MTJMSD to harness the molecules as the device element. MCS study provides a representative understanding of the equilibrium properties of MTJMSD evolving due to the variations in anisotropies at different thermal energies.

ACKNOWLEDGEMENT: This research is supported by National Science Foundation-CREST Award (Contract # HRD- 1914751), Department of Energy/ National Nuclear Security Agency (DE-FOA-0003945).

Author Contributions Statement: Bishnu Dahal conducted simulations studies, Andrew Grizzle developed analysis software to analyze the data, and Christopher D'Angelo wrote a C++ MCS program under the supervision of Pawan Tyagi. Pawan Tyagi conducted experimental studies. Vincent Lamberti contributed in data analysis. Pawan Tyagi and Bishnu Dahal wrote the manuscript and analyzed the data.

Data availability statement: The data supporting this study's findings are available within the article [and its supplementary material]. The additional data supporting this study's findings are available from the corresponding author upon reasonable request.

Conflicts of Interest Statement: The authors whose names are listed immediately below certify that they have NO affiliations with or involvement in any organization or entity with any financial interest (such as honoraria; educational grants; participation in speakers' bureaus; membership, employment, consultancies, stock ownership, or other equity interest; and expert testimony or patent-licensing arrangements), or non-financial interest (such as personal or professional relationships, affiliations, knowledge or beliefs) in the subject matter or materials discussed in this manuscript.

References:

1. Peng, S., et al., *Magnetic Tunnel Junctions for Spintronics: Principles and Applications.* Wiley Encyclopedia of Electrical and Electronics Engineering.
2. Zhu, J.-G.J. and C. Park, *Magnetic tunnel junctions.* Mat. Today, 2006. **9**(11): p. 36-45.
3. Yao, X., et al., *Magnetic tunnel junction-based spintronic logic units operated by spin transfer torque.* IEEE Trans. Nanotech., 2012. **11**(1): p. 120-126.
4. Bader, S. and S. Parkin, *Spintronics.* Annu. Rev. Condens. Matter Phys., 2010. **1**(1): p. 71-88.
5. Bhatti, S., et al., *Spintronics based random access memory: a review.* Materials Today, 2017. **20**(9): p. 530-548.
6. Sanvito, S. and A.R. Rocha, *Molecular-spintronics: The art of driving spin through molecules.* Journal of Computational and Theoretical Nanoscience, 2006. **3**(5): p. 624-642.
7. Lyle, A., et al., *Magnetic tunnel junction logic architecture for realization of simultaneous computation and communication.* IEEE Trans. Magn., 2011. **47**(10): p. 2970-2973.
8. Gallagher, W.J., et al., *Magnetic tunnel junctions with controlled magnetic response*, 1997, Google Patents.
9. Maciel, N., et al., *Magnetic tunnel junction applications.* Sensors, 2020. **20**(1): p. 121.
10. Yuasa, S., et al., *Giant room-temperature magnetoresistance in single-crystal Fe/MgO/Fe magnetic tunnel junctions.* Nature Materials, 2004. **3**(12): p. 868-71.
11. Coronado, E. and A.J. Epsetin, *Molecular spintronics and quantum computing.* J. Mater. Chem., 2009. **19**(12): p. 1670-1671.
12. Coronado, E., et al., *Design of molecular materials combining magnetic, electrical and optical properties.* Journal of the Chemical Society, Dalton Transactions, 2000(21): p. 3955-3961.
13. Cornia, A. and P. Seneor, *SPINTRONICS The molecular way.* Nature Materials, 2017. **16**(5): p. 505-506.
14. Pasupathy, A.N., et al., *The Kondo effect in the presence of ferromagnetism.* Science, 2004. **306**(5693): p. 86-89.
15. Tyagi, P., *Multilayer Edge Molecular Electronics Devices: A Review.* J. Mater. Chem., 2011. **21**(13): p. 4733-4742.
16. Affronte, M., et al., *Single molecule magnets for quantum computation.* J. Phys. D-Appl. Phys., 2007. **40**(10): p. 2999-3004.
17. Tomsa, A.-R., et al., *A new family of oxime-based hexanuclear manganese (III) single molecule magnets with high anisotropy energy barriers.* Chem. Comm., 2010. **46**(28): p. 5106-5108.
18. Voss, S., et al., *Identification of linker molecules suited for deposition and study of Mn-12 single molecule magnets on Au surfaces.* J. Appl. Phys., 2008. **103**: p. 07B901.
19. Coronado, E. and M. Yamashita, *Molecular spintronics: the role of coordination chemistry.* Dalton Transactions, 2016. **45**(42): p. 16553-16555.
20. Sanvito, S., *Molecular spintronics.* Chemical Society Reviews, 2011. **40**(6): p. 3336-3355.
21. Tyagi, P., C. Baker, and C. D'Angelo, *Paramagnetic molecule induced strong antiferromagnetic exchange coupling on a magnetic tunnel junction based molecular spintronics device.* Nanotechnology, 2015. **26**(30): p. 305602.
22. Savadkoohi, M., et al., *Interaction between magnetic molecules and two ferromagnetic electrodes of a magnetic tunnel junction (MTJ).* Journal of Magnetism and Magnetic Materials, 2021. **529**: p. 167902.
23. Tyagi, P. and E. Friebe, *Large Resistance Change on Magnetic Tunnel Junction based Molecular Spintronics Devices.* J. Mag. Mag. Mat., 2018. **453**: p. 186-192.

24. Yu, A.C., et al., *Effect of Ti seed layer on the magnetization reversal process of Co/NiFe/Al-oxide/NiFe junction films.* J. App. Phys., 2002. **91**(8): p. 5234-5239.
25. Yu, C. and A. Petford-Long, *Effect of ferromagnetic layer structure on the magnetization process in NiFe/Co/Al–O/NiFe and Co/NiFe/Al–O/NiFe junctions.* J. App. Phys., 1999. **85**(8): p. 5753-5755.
26. Yu, G.H., et al., *Dead layer in a Ta/Ni81Fe19/Ta structure.* Chinese Physics Letters, 2002. **19**(9): p. 1347-1349.
27. Yu, G.H., et al., *Interface reaction of Ta/Ni81Fe19 or Ni81Fe19/Ta and its suppression.* App. Phys. Lett., 2002. **80**(3): p. 455-457.
28. Dubowik, J., et al., *Anisotropy Distribution in NiFe/Au/Co/Au Multilayers.* Acta Physica Polonica-Series A General Physics, 2009. **115**(1): p. 315.
29. Tyagi, P., C. Baker, and C. D'Angelo, *Paramagnetic Molecule Induced Strong Antiferromagnetic Exchange Coupling on a Magnetic Tunnel Junction Based Molecular Spintronics Device.* Nanotechnology, 2015. **26**: p. 305602.
30. Li, D.F., et al., *An S=6 cyanide-bridged octanuclear (Fe4Ni4II)-Ni-III complex that exhibits slow relaxation of the magnetization.* J. Am. Chem. Soc., 2006. **128**(13): p. 4214-4215.
31. Li, D.F., et al., *Ancillary Ligand Functionalization of Cyanide-Bridged S = 6 FeIII4NiII4 Complexes for Molecule-Based Electronics.* Inorg. Chem., 2006. **45**(13): p. 7569.
32. Tyagi, P. and C. Riso, *Molecular spintronics devices exhibiting properties of a solar cell.* Nanotechnology, 2019. **30**(49): p. 495401.
33. Tyagi, P., C. Riso, and E. Friebe, *Magnetic Tunnel Junction Based Molecular Spintronics Devices Exhibiting Current Suppression At Room Temperature.* Organic Electronics, 2019. **64**: p. 188-194.
34. Kuekes, P.J., G.S. Snider, and R.S. Williams, *Crossbar nanocomputers.* Scientific American, 2005. **293**(5): p. 72-80.
35. Tyagi, P. and C. Riso, *Magnetic force microscopy revealing long range molecule impact on magnetic tunnel junction based molecular spintronics devices.* Organic Electronics, 2019. **75**: p. 105421.
36. Dahal, B.R., et al., *Easy axis anisotropy creating high contrast magnetic zones on magnetic tunnel junctions based molecular spintronics devices (MTJMSD).* Scientific reports, 2022. **12**(1): p. 1-14.
37. Johnson, M., *Magnetoelectronics*. 2004: Academic Press.
38. Bennemann, K., *Magnetic nanostructures.* J. Phys. Cond. Mat., 2010. **22**(24).
39. Grizzle, A., et al., *Spin state of a single-molecule magnet (SMM) creating long-range ordering on ferromagnetic layers of a magnetic tunnel junction – a Monte Carlo study.* RSC Advances, 2021. **11**(51): p. 32275-32285.
40. O'handley, R.C., *Modern magnetic materials: principles and applications*. 1999: Wiley Inter-Science.